Research Article

Luteolin delays photoreceptor degeneration in a mouse model of retinitis pigmentosa

https://doi.org/10.4103/1673-5374.303537
Date of submission: September 2, 2020
Date of decision: November 2, 2020
Date of acceptance: December 24, 2020
Date of web publication: February 19, 2021

Xiao-Bin Liu[1], Feng Liu[1], Yi-Yao Liang[1], Gang Yin[2], Hui-Jun Zhang[3], Xue-Song Mi[3], Zai-Jun Zhang[2], Kwok-Fai So[1, 4, 5], Ang Li[1, 4, *], Ying Xu[1, 5, *]

Graphical Abstract *Mechanisms of luteolin on protecting photoreceptors*

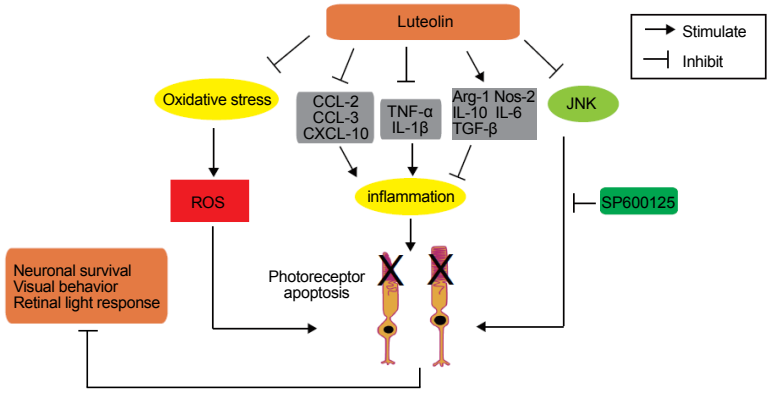

Abstract

Luteolin is neuroprotective for retinal ganglion cells and retinal pigment epithelial cells after oxidative injury, whereby it can inhibit microglial neurotoxicity. Therefore, luteolin holds the potential to be useful for treatment of retinal diseases. The purpose of this study was to investigate whether luteolin exhibits neuroprotective effects on rod cells in rd10 mice, a slow photoreceptor-degenerative model of retinitis pigmentosa. Luteolin (100 mg/kg) intraperitoneally injected daily from postnatal day 14 (P14) to P25 significantly enhanced the visual performance and retinal light responses of rd10 mice at P25. Moreover, it increased the survival of photoreceptors and improved retinal structure. Mechanistically, luteolin treatment attenuated increases in reactive oxygen species, photoreceptor apoptosis, and reactive gliosis; increased mRNA levels of anti-inflammatory cytokines while lowering that of pro-inflammatory and chemoattractant cytokines; and lowered the ratio of phospho-JNK/JNK. Application of the JNK inhibitor SP600125 exerted a similar protective effect to luteolin, suggesting that luteolin delays photoreceptor degeneration and functional deterioration in rd10 mice through regulation of retinal oxidation and inflammation by inhibiting the JNK pathway. Therefore, luteolin may be useful as a supplementary treatment for retinitis pigmentosa. This study was approved by the Qualified Ethics Committee of Jinan University, China (approval No. IACUC-20181217-02) on December 17, 2018.

Key Words: anti-inflammation; apoptosis; flavonoid; JNK pathway; luteolin; photoreceptor; reactive gliosis; reactive oxygen species; retinal degeneration; retinitis pigmentosa

Chinese Library Classification No. R453; R774.6; Q429+.2

Introduction

Retinitis pigmentosa (RP) is a hereditary retinal dystrophic disorder that results from progressive losses of rods and cones, which ultimately causes blindness (Hartong et al., 2006). Although RP affects approximately 1 out of 4000 people globally, so far there are no effective treatments. Many approaches have been employed to delay the degeneration of photoreceptors, such as antioxidants, anti-inflammatory reagents (Zhang et al., 2017; Liu et al., 2018), transcription or nutrition factors (Azadi et al., 2007; Jiang et al., 2014), and histone deacetylase inhibitors (Trifunović et al., 2016). Among nutritional supplements, various types of flavonoids have demonstrated neuroprotective roles in models of retinal degenerative diseases including diabetic retinopathy (Rossino and Casini, 2019), age-related macular degeneration (Pawlowska et al., 2019), and RP (Head, 1999; Herrera-

[1]Guangdong-Hong Kong-Macau Institute of CNS Regeneration, Ministry of Education CNS Regeneration Collaborative Joint Laboratory, Jinan University, Guangzhou, Guangdong Province, China; [2]Institute of New Drug Research and Guangzhou Key Laboratory of Innovative Chemical Drug Research in Cardio-cerebrovascular Diseases, Jinan University, Guangzhou, Guangdong Province, China; [3]Department of Ophthalmology, the First Affiliated Hospital of Jinan University, Guangzhou, Guangdong Province, China; [4]Bioland Laboratory (Guangzhou Regenerative Medicine and Health Guangdong Laboratory), Guangzhou, Guangdong Province, China; [5]Co-Innovation Center of Neuroregeneration, Nantong University, Nantong, Jiangsu Province, China.
*Correspondence to: Ying Xu, PhD, xuying@jnu.edu.cn; Ang Li, PhD, anglijnu@jnu.edu.cn.
https://orcid.org/0000-0002-9987-2057 (Ying Xu); https://orcid.org/0000-0002-9886-4880 (Ang Li)

Funding: *The work was supported by the National Natural Science Foundation of China, Nos. 81470656 (to YX), 82071372 (to AL), 82074169 (to XSM); Guangdong Grant Key Technologies for Treatment of Brain Disorders', China, No. 2018B030332001 (to YX); Ningxia Key Research and Development Program Grant (Yinchuan, Ningxia Hui Autonomous Region, China) (to KFS); Program of Introducing Talents of Discipline to Universities, China, No. B14036 (to YX, AL, KFS); Outstanding Scholar Program of Bioland Laboratory (Guangzhou Regenerative Medicine and Health Guangdong Laboratory), No. 2018GZR110102002 (to KFS, AL); and Science and Technology Program of Guangzhou, No. 202007030012 (to KFS and AL).*
How to cite this article: *Liu XB, Liu F, Liang YY, Yin G, Zhang HJ, Mi XS, Zhang ZJ, So KF, Li A, Xu Y (2021) Luteolin delays photoreceptor degeneration in a mouse model of retinitis pigmentosa. Neural Regen Res 16(10):2109-2120.*

Hernández et al., 2017).

Luteolin (3′,4′,5,7-tetrahydroxyflavone; **Figure 1A**) is an important flavonoid present in numerous plants, such as vegetables, fruits, and medicinal herbs. With its capacity to scavenge both oxygen and nitrogen species, luteolin exerts many biological effects including anti-oxidation (Williams et al., 2004), anti-inflammation (Chen et al., 2007), and anti-angiogenesis (Park et al., 2012). In the eye, luteolin was shown to be neuroprotective following oxidative injury of retinal ganglion cells (Maher and Hanneken, 2005) and retinal pigment epithelial cells (Hanneken et al., 2006; Hytti et al., 2015). In an *in vitro* experiment, luteolin was found to inhibit microglial neurotoxicity (Dirscherl et al., 2010). These properties of luteolin indicate that it may be useful for treating other retinal diseases.

In Pde6b^{rd10} (rd10) mice, a canonical model of RP, rod cells begin to degenerate around postnatal day 18 (P18) due to a mutation of the *Pde6b* gene encoding rod phosphodiesterase (Chang et al., 2007), which also causes RP in human patients. The death of rods peaks around P25 and is almost completed by P45 (Gargini et al., 2007). We hypothesized that luteolin might delay photoreceptor degeneration in rd10 mice as a result of its anti-oxidative and anti-inflammatory properties. In this study, we asked whether luteolin could protect retinal photoreceptors and delay their degeneration in rd10 mice.

Materials and Methods

Animals

rd10 (Pde6b^{rd10}) and wild-type (WT) (C57BL/6J) mice (aged 8–10 weeks, of either gender, weighing 15–20 g) were purchased from Jackson Laboratory (Bar Harbor, ME, USA) and the Experimental Animal Center of Guangdong Province [License No. SCXK (Yue) 2018-0002; Guangzhou, China], respectively. All animals were housed under standard conditions (25°C room temperature, 40–60% humidity, 12-hour light/dark cycle) and allowed free access to food and water. Animal experiments were conducted according to the Association for Research in Vision and Ophthalmology Statement for the Use of Animals in Ophthalmic and Visual Research, and approved by the Qualified Ethics Committee of Jinan University (approval No. IACUC-20181217-02) on December 17, 2018. All efforts were made to minimize the number of mice utilized and their suffering.

Measurement of luteolin concentrations in the mouse retina

Luteolin (CAS: 491-70-3; molecular weight 286.23 Da) purchased from Mansite Biotechnology Co., Ltd. (Chengdu, China), was first dissolved in 1 N NaOH and then the pH of the stock solution was adjusted to 7.2 with 1 N HCl. Thereafter, the stock was further diluted with phosphate-buffered saline (PBS, 0.01 M) (Hendriks et al., 2004).

High-performance liquid chromatography was applied to determine whether and how much luteolin could reach the retina. Luteolin (100 mg/kg body weight) (Hendriks et al., 2004; Ziyan et al., 2007; Liu et al., 2013) was intraperitoneally (i.p.) injected into 4- to 5-week-old WT mice. After 15, 30, or 60 minutes, mice were euthanized by dislocation of cervical vertebra and retinas were extracted. For each time point, proteins from six retinas of three mice were pooled and processed using a previously reported protocol (Xiang et al., 2018), with the ultraviolet detection wavelength set at 350 nm.

Study design

Animals were randomly assigned to five groups: WT (n = 46), PBS (rd10 + PBS; n = 58), luteolin (rd10 + luteolin; n = 64), dimethyl sulfoxide (rd10 + dimethyl sulfoxide; n = 4), and SP600125 (rd10 + SP600125; n = 4). Concentrations of luteolin ranging from 50–120 mg/kg body weight (Hendriks et al., 2004; Ziyan et al., 2007; Liu et al., 2013) or equal volumes of PBS were i.p. injected daily into rd10 littermates starting from P14 (after eye opening) until P25 (when photoreceptor apoptosis peaks) (Gargini et al., 2007; Barhoum et al., 2008). At P25, rd10 mice were examined for their visual behaviors using the black and white transition, and optomotor tests. Thereafter, mice were dark-adapted overnight and an electroretinogram (ERG) recording was performed the next day (P26), followed by immediate sacrifice and tissue collection. Retinas were subjected to either immunochemical staining or total RNA and protein extraction for subsequent real-time quantitative polymerase chain reaction (RT-qPCR) and western blot assays, respectively. To examine the long-term impacts of treatments, several assessments were performed at P45, a point at which most rods have degenerated. Age-matched WT mice were simultaneously tested along with normal controls. The detailed protocol is illustrated in **Figure 1B**.

In another set of experiments, the c-Jun N-terminal kinase (JNK) antagonist SP600125 (Sigma-Aldrich, St. Louis, MO, USA) was dissolved in dimethyl sulfoxide (DMSO; Sigma-Aldrich) at a concentration of 20 mg/mL, diluted in PBS, and i.p. injected into rd10 mice at a dosage of 15 mg/kg body weight (Shen et al., 2017) from P14 to P25, when the mice were sacrificed. Diluted DMSO was used as a control for the SP600125 group.

Visual behavioral tests

Visual behavioral tests were performed at P25 by virtue of both the dark-light transition test and a homemade optomotor system. The dark-light transition test, which measures the tendency of a mouse to stay in darkness rather than an illuminated area, was carried out as previously described (Zhang et al., 2017; Xiang et al., 2018). In brief, a mouse was placed in the center of a light chamber (Metronet Technology Ltd., Beijing, China) that connects to a dark chamber, and allowed to move freely between the chambers. Movements were recorded and the duration each mouse spent in the dark chamber during a 5-minute test was automatically quantified by EthoVision XT 8.0 software (Noldus, Wageningen, Netherlands), and the percentage against total duration of the test (5 minutes) was calculated.

The optomotor test measures visual acuity by observing head turning in response to moving gratings (Prusky et al., 2004). A free-moving mouse was placed on a platform in the middle of an arena circled by four computer monitors displaying vertical sine wave gratings with 100% contrast written with MATLAB (MathWorks, Natick, MA, USA). Spatial frequencies examined included 0.1, 0.15, 0.2, 0.25, 0.3, 0.35, 0.4, and 0.45 cycles/degree at a constant speed of 12 degrees/s; gratings with each spatial frequency were rotated clockwise for 1 minute and then counterclockwise for 1 minute. Animals reflexively track the gratings by moving their head as long as they could see them. Head movements were videotaped and the maximal spatial frequency at which an optomotor response could be observed was manually recorded to reflect visual acuity of a mouse.

ERG

To measure light responses of retinal neurons, mice were dark-adapted overnight after behavioral tests, and their retinal function was assessed with a RETIscan System (Roland Consult, Brandenburg, Germany), as previously described (Yang et al., 2015; Zhang et al., 2017). Dark-adapted mice were stimulated with green flashes of increasing intensities (0.01, 0.1, and 3.0 cd·s/m^2) and photopic responses to green flashes of 10.0 cd·s/m^2 were recorded. For each mouse, the value from the eye that produced a larger response at scotopic 3.0 cd·s/m^2 was taken as the reading.

Tissue processing and immunofluorescence

After the ERG test, mice were euthanized by anesthetic

overdose (i.p. injection of 100 mg/kg pentobarbital sodium; R&D Systems, Minneapolis, MN, USA), and their eyes were enucleated and fixed in 4% paraformaldehyde at room temperature for 30 minutes. Thereafter, the eyes were rinsed three times with PBS for 5 minutes each, cryoprotected overnight in 0.01 M PBS containing 30% sucrose at 4°C, and ultimately embedded in Optimal Cutting Temperature Compound (Tissue-Tek, Torrance, CA, USA). Retinas were cryosectioned on a microtome (Leica Microsystems, Buenos Aires, Argentina) through the optic disk longitudinally at a thickness of 10 µm. Thereafter, retinal sections were mounted on glass slides for further processing.

For immunofluorescence staining, samples were washed three times with 0.01 M PBS before incubating in 0.01 M PBS containing 10% normal donkey serum, 3% bovine serum albumin, and 0.3% Triton X-100 for 1 hour, followed by primary antibodies overnight at 4°C. After thorough washing, retinal sections were probed with secondary antibodies for 2 hours at room temperature, subsequently washed, mounted, and coverslipped. To visualize cell nuclei, sections were treated with 4′,6-diamidino-2-phenylindole (DAPI; 1:1000, Electron Microcopy Sciences, Hatfield, PA, USA) for 5 minutes prior to mounting.

Primary antibodies included mouse anti-rhodopsin (1:500, Cat# MAB5356, Millipore, Bedford, MA, USA), mouse anti-red/green opsin (1:500, Cat# AB5405, Millipore), rat anti-glial fibrillary acidic protein (GFAP; 1:500, Cat# 13-0300, Thermo Fisher Scientific, Waltham, MA, USA), rabbit anti-ionized calcium-binding adapter molecule 1 (Iba1; 1:1000, Cat# 019-19741, Wako, Osaka, Japan), and rabbit anti-protein kinase C-α (1:200, Cat# p4334, Sigma-Aldrich), for staining the rod outer segment, cone outer segment, Müller cell processes, microglia and rod bipolar cells, respectively. Secondary antibodies included donkey anti mouse IgG conjugated to Alexa Fluor-488 (1:1000, Cat#150105), donkey anti mouse IgG conjugated to Alexa Fluor-594 (1:1000, Cat#150108), donkey anti-rabbit IgG conjugated to Alexa Fluor-488 (1:1000, Cat#150073) and goat anti-rat IgG conjugated to Alexa Fluor-488 (1:1000, Cat#150165; all from Abcam, Cambridge, UK).

To identify apoptotic retinal neurons, we applied a terminal deoxynucleotidyl transferase dUTP nick end-labeling (TUNEL) assay (In Situ Cell Death Detection Kit; Roche Applied Science, Indianapolis, IN, USA), as previously described (Zhang et al., 2017). To assay reactive oxygen species (ROS) production in the retina, cryosections from freshly fixed retinas were incubated with 5 µM dihydroethidium (DHE, Cat# BB-47051, BestBio Inc., Shanghai, China) in PBS for 30 minutes at 37°C. DHE specifically reacts with superoxide anions and converts to ethidium, which gives off red fluorescence. To compare DHE fluorescence intensities, tissues from each group were processed in parallel using identical procedures and imaging parameters.

Image collection and processing

Tissues stained with DAPI alone were captured with a fluorescence microscope (Carl Zeiss, Oberkochen, Germany), while others were captured with a confocal microscope (Carl Zeiss LSM700). Considering that photoreceptors of rd10 mice degenerate from the center to the periphery, we compared structures of the same eccentricity at 1.0 mm away from the optic disk center (Wang et al., 2014; Zhang et al., 2017). The thickness of the outer nuclear layer (ONL) was quantified using the DAPI-stained sections. To quantify lengths of the cone outer segment or Müller cell processes, a line was drawn along the axis of each cone outer segment stained with anti-R/G opsin or Müller cell process stained with anti-GFAP antibody; the lengths of these lines were then averaged for each image. The thickness of rod outer segments was defined as the thickness of the layer stained with anti-rhodopsin. Lengths of bipolar cell dendrites were determined by drawing a line from the top of a soma to the end of the longest dendrite of that cell; at least 10 cells were included for each image. To count the number of activated Müller cells, for each section (320 µm × 320 µm), we counted GFAP-positive processes that vertically ran across the inner nuclear layer. Iba1 expression and DHE staining were quantified as the Iba1-positive fluorescent area and average fluorescent intensity of DHE across the whole retina, respectively. All measurements were analyzed with ImageJ software (National Institutes of Health, Bethesda, MD, USA). For each retina, values from 3–6 images were averaged to provide one data point, and all of the data points from retinas of a group were further averaged to obtain the mean value.

Protein array detection

Protein array detection was applied to screen for possible signaling pathways modulated by luteolin. Total proteins were extracted from homogenized retinas at P25 (for C57, PBS, and luteolin groups: both retinas from five, three, and three mice were used for the first experiment; and five, four, and three mice for the second experiment, respectively) and adjusted to a final concentration of 2 mg/mL. Expression levels of phosphorylated proteins were detected by Human/Mouse Mitogen-Activated Protein Kinase (MAPK) and Protein Kinase B (PKB/AKT) Pathway Phosphorylation Arrays (RayBiotech, Peachtree Corners, GA, USA), in a semiquantitative way. Following protocols recommended by the manufacturer, each array membrane was pretreated with blocking buffer at room temperature for 30 minutes, followed by incubation with 400 µg of the protein sample overnight at 4°C. After adequate washing, the Detection Antibody Cocktail together with a horseradish peroxidase (HRP)-conjugated anti-rabbit IgG reagent were sequentially applied to each membrane and reacted overnight at 4°C. Thereafter, the Detection Buffer Mixture was applied to the membrane and the chemiluminescence signal was captured within 10–15 minutes using a gel documentation system (ChemiTouch, Bio-Rad Laboratories, Hercules, CA, USA). The intensity of dots was quantified and compared with Image J software. Fold changes within the range of 0.7–1.3 were regarded as insignificant.

Western blot assay

For western blot, 30 µg of retinal proteins were loaded in each lane and separated by electrophoresis on 12% (v/v) sodium dodecyl sulphate-polyacrylamide gels, and then transferred to polyvinylidene difluoride membranes (Millipore). Membranes were incubated with PBS containing 5% dried non-fat milk for 1.5 hours at room temperature and then probed with primary antibodies including rabbit anti-JNK (1:1000, Cat# 9252), anti-phosphorylated (p-) JNK (1:1000, Cat# 4668), anti-extracellular-signal-regulated kinase (ERK; 1:1000, Cat# 9102), anti-p-ERK (1:2000, Cat# 4370), and anti-glyceraldehyde 3-phosphate dehydrogenase (1:5000, Cat# 2118; all from Cell Signaling Technologies, Danvers, MA, USA) at 4°C overnight. After incubation with goat anti-rabbit horseradish peroxidase-conjugated IgG (1:5000, Cat# 111-035-003, Jackson ImmunoResearch, West Grove, PA, USA) for 1.5 hours at room temperature, blots were washed three times with PBS and incubated with an enhanced chemiluminescence reagent (Bio-Rad Laboratories). Image documentation, processing, and quantification were similarly performed with ImageJ software as mentioned above. A ratio for the total intensity of the target protein over that of the loading control was calculated and normalized to WT group. Measurements were repeated for at least 3 times in each experiment.

Real-time quantitative PCR (RT-qPCR)

Dynamic alterations of gene expression of inflammation-related factors were measured by RT-qPCR, as previously described (Sun et al., 2017). In brief, retinas from each mouse were isolated and lysed in TRIzol (Thermo Fisher

Scientific) with a handheld homogenizer. Following a 5-minute incubation, chloroform was added to the homogenate. The mixture was vigorously shaken for 15 seconds and then centrifuged at 14,000 × *g* for 15 minutes at 4°C. Thereafter, the uppermost aqueous phase was mixed with an equal volume of ethanol (70%) and subjected to processing with a Total RNA Purification System (Cat# 12183018A, Thermo Fisher Scientific) according to the manufacturer's instructions. Complementary DNA (cDNA) templates were synthesized using the MightyScript Plus First Strand cDNA Synthesis Master Mix (Sangon Biotech, Shanghai, China). Real-time PCR detection with gene-specific primers (IDT, Coralville, IA, USA; **Table 1**) and TB Green Premix Ex Taq II-Tli RNaseH Plus (Takara, Dalian, China) was carried out as previously reported (Sun et al., 2017). Assays were run on an Eco Real-Time PCR System (Illumina, San Diego, CA, USA) using the following ramping protocol: 95°C for 45 seconds, followed by 50 cycles of 95°C for 5 seconds and 60°C for 30 seconds. Relative quantities of gene transcripts were calculated according to the $2^{-\Delta\Delta CT}$ method and normalized to WT controls, using mouse *β-actin* as the housekeeping gene.

Table 1 | **Real-time polymerase chain reaction primers for quantification of gene expression**

Target	Sequence (5' to 3')
Il-1ß	Sense: GAC CTG TTC TTT GAA GTT GAC G
	Anti-sense: CTC TTG TTG ATG TGC TGC TG
Tnf-α	Sense: AGA CCC TCA CAC TCA GAT CA
	Anti-sense: TCT TTG AGA TCC ATG CCG TTG
Arg-1	Sense: GAA TGG AAG AGT CAG TGT GGT
	Anti-sense: AGT GTT GAT GTC AGT GTG AGC
Tgf-ß1	Sense: GCG GAC TAC TAT GCT AAA GAG G
	Anti-sense: CCG AAT GTC TGA CGT ATT GAA GA
Nos2	Sense: GAC TGA GCT GTT AGA GAC ACT T
	Anti-sense: CAC TTC TGC TCC AAA TCC AAC
Il-10	Sense: GTC ATC GAT TTC TCC CCT GTG
	Anti-sense: ATG GCC TTG TAG ACA CCT TG
Il-6	Sense: AGC CAG AGT CCT TCA GAG A
	Anti-sense: TCC TTA GCC ACT CCT TCT GT
Ccl-3	Sense: CCT TGC TGT TCT TCT CTG TAC C
	Anti-sense: CGA TGA ATT GGC GTG GAA TC
Ccl-2	Sense: CAT CCA CGT GTT GGC TCA
	Anti-sense: AAC TAC AGC TTC TTT GGG ACA
Cxcl-10	Sense: ATT TTC TGC CTC ATC CTG CT
	Anti-sense: TGA TTT CAA GCT TCC CTA TGG C
Actb	Sense: GGC TGT ATT CCC CTC CAT CG
	Anti-sense: CCA GTT GGT AAC AAT GCC ATG T

Actb: β-Actin; Arg-1: arginase 1; Ccl: C-C motif chemokine ligand; Cxcl: CXC motif chemokine ligand; Il: interleukin; Nos2: nitric oxide synthase 2; Tgf-β1: transforming growth factor β1; Tnf-α: tumor necrosis factor α.

Statistical analysis

All data are presented as mean ± standard error of mean (SEM). Prism 7 (GraphPad Software, San Diego, CA, USA) was utilized for statistical analysis. Statistical significance of parametric data was determined with Student's *t*-test or one-way analysis of variance with Tukey's *post hoc* test, as appropriate. *P* values < 0.05 and < 0.01 were considered significant and highly significant, respectively.

Results

Luteolin rapidly enters the retina following i.p. injection

To examine whether luteolin could cross the blood-retina barrier after i.p. administration, we measured its concentration in retinas harvested 15, 30, and 60 minutes after i.p. injection at a dosage of 100 mg/kg body weight. Luteolin became detectable in the retina 15 minutes after i.p. administration, with corresponding levels of 26.06 μg/mL and 8.44 μg/mL at 15 and 30 minutes, respectively. At 60 minutes, the concentration decreased to 2.82 μg/mL (i.e. 9.7 μM). As luteolin demonstrates a strong anti-oxidative effect on cultured retinal cells at 10 μM (Maher and Hanneken, 2005), we considered injection of ~100 mg/kg to be appropriate for testing potential biological effects on the retina *in vivo*.

Optimizing the dosage of luteolin for i.p. injection

We next explored the optimal dosage of luteolin (ranging from 50 to 120 mg/kg body weight) following a daily single i.p. injection from P14 to P25. As a simple index of rod survival, we used thickness of the ONL at 1.0–1.3 mm away from the optic nerve center (Wang et al., 2014). Our results show that following injection of 100 mg/kg luteolin, average thickness of the ONL was 2.0 ± 0.1-fold greater than that of the PBS group. Moreover, it was greater than that of the groups receiving 50 mg/kg (1.2 ± 0.2-fold) or 120 mg/kg (1.6 ± 0.1-fold) luteolin (**Figure 1C**). Therefore, for the remaining experiments, we applied luteolin at a dosage of 100 mg/kg.

Luteolin improves visual behaviors in rd10 mice

To investigate whether luteolin enhanced the visual function of rd10 mice, we tested their light perception using the dark-light transition, and their visual acuity using optomotor responses. The dark-light transition box (**Figure 2A**) can evaluate the perception of luminance by a mouse's tendency to stay in darkness, as WT mice with normal vision tend to spend most of their time in the dark chamber. At P26, the time that PBS-treated rd10 mice spent in darkness was substantially reduced (43.0 ± 2.7% of the total duration, *n* = 12) compared with WT mice (65.2 ± 2.3%, *n* = 10, *P* < 0.001), indicating an impaired capability to detect luminance. Following luteolin treatment, rd10 mice stayed substantially longer in darkness (64.3 ± 2.7%, *n* = 14, *P* < 0.001, *vs*. PBS-treated controls; **Figure 2B**).

Optomotor responses indicate the visual acuity of a mouse by exposing it to moving gratings of increasing spatial frequencies (**Figure 2C**) (Prusky et al., 2004). The higher the spatial frequency (i.e. the finer the grating) that an animal can respond to, the greater its visual acuity. Compared with WT mice, which detected 0.36 ± 0.01 cycles/degree (*n* = 7), the threshold of rd10 mice was much lower (0.18 ± 0.02 cycles/degree, *n* = 11, *P* < 0.001). Luteolin treatment significantly improved visual acuity according to this index, which increased to 0.30 ± 0.01 cycles/degree (*n* = 11, *P* < 0.001, *vs*. PBS-treated group; **Figure 2D**). However, rd10 mice tested at P45 hardly showed any improvement (**Additional Figure 1A**). Thus, amelioration of visual behaviors in rd10 mice by luteolin seemed to be restricted to an early stage of degeneration.

Luteolin enhances the retinal light response of rd10 mice

To examine the impact of luteolin on retinal physiology, ERG recordings were performed at P26. In WT mice, retinal neurons responded well to light flashes under both dark-adapted (black lines in **Figure 3A**) and light-adapted (photopic) conditions (**Figure 3C**). Owing to photoreceptor degeneration, light responses in rd10 mice were dramatically decreased (gray lines in **Figure 3**), but could be partly recovered by luteolin (gray dotted lines in **Figure 3**). Under dark-adapted conditions, the average amplitudes of a- and b-waves at 3.0 cd·s/m^2 in PBS-treated rd10 mice (*n* = 8) were significantly reduced compared with those of WT controls (*P* < 0.001, *n* = 11). Following luteolin treatment, a- and b-wave amplitudes were both significantly increased [2-fold for a-wave (*P* < 0.05) and 3.2-fold for b-wave (*P* < 0.001), *n* = 9; **Figure 3B**)]. At lower flash intensities of 0.01 and 0.1 cd·s/m^2, luteolin tended to increase amplitudes of both a- and b-waves, but there was no significant difference compared with the PBS-treated group (**Additional Figure 2**).

Under photopic conditions, the a-wave amplitude slightly

declined, which was partially recovered by luteolin (**Figure 3D**). The photopic b-wave amplitude decreased significantly from 76.5 ± 10.4 μV in WT controls to 23.9 ± 9.0 μV in PBS-treated rd10 mice (P < 0.01). Luteolin treatment markedly increased the b-wave amplitude to 54.8 ± 6.2 μV (P < 0.05, *vs*. PBS-treated group; **Figure 3D**). Hence, our ERG results indicate that luteolin preserved both rod- and cone-mediated light responses in the rd10 retina.

Consistent with the results of visual behavioral tests, luteolin improved neither scotopic nor photopic ERG responses at P45 (**Additional Figure 1B** and **C**).

Luteolin preserves retinal structures in rd10 mice

Improvements in scotopic and photopic ERG after luteolin treatment suggest that photoreceptor and/or bipolar cell degeneration was slowed down. Thus, the survival of photoreceptors was examined at different eccentricities from the central to peripheral regions. Typical examples of retinal slices from the middle region of each group are shown in **Figure 4A**. By P25, the ONL thickness in PBS-treated rd10 retinas became considerably thinner at all regions (P < 0.001, *vs*. WT counterparts). In the luteolin-treated group, more layers of photoreceptor somas remained and the ONL was significantly thicker (1.2–1.5-fold) compared with the PBS-treated group (**Figure 4B**; P < 0.05 at 800 μm and 1200 μm from the center). At P45, when rod degeneration enters the late stage, only a single tier of somas remained in the ONL of PBS-treated rd10 retinas, and luteolin had little effect (**Additional Figure 1D**).

We next studied the structure of cone and rod photoreceptors by immunostaining. In WT retina, staining for rhodopsin at P25 was very strong in the outer segments, but weak in the inner segments and somas. In PBS-treated rd10 retina, staining was predominantly restricted to the outer segments that had become much shorter (**Figure 5A**, left and middle panel). After luteolin treatment, the outer segment layer was thicker, indicating longer outer segments (7.3 ± 2.2 μm *vs*. 3.4 ± 0.7 μm in PBS group, P < 0.01; **Figure 5B**). Similarly, staining for red/green opsin in WT retina revealed clear long cone outer segments (14.4 ± 0.6 μm; **Figure 5C**), which were significantly shortened in PBS-treated rd10 mice (2.2 ± 0.1 μm) but dramatically restored with luteolin administration (6.4 ± 0.8 μm, P < 0.01; **Figure 5D**).

To evaluate protection of retinal structures by luteolin, we assessed the structures of rod bipolar cells with an antibody against protein kinase C-α (**Figure 5E**). As the dendritic trees of bipolar cells shrink upon the loss of their synaptic input, measuring dendritic length can indicate the ability of these cells to collect information. In the rd10 retina, dendritic length was 48% of WT controls (**Figure 5E**). The average length of these dendrites was significantly increased from 5.4 ± 0.2 μm in the PBS-treated group to 8.2 ± 0.3 μm (or 72% of WT controls) in the luteolin-treated group (P < 0.01; **Figure 5F**). Collectively, our results indicate that luteolin had a protective effect on the retinal structure of rd10 mice.

Luteolin reduces apoptosis and oxidative stress in retinas of rd10 mice

Having identified the protective effect of luteolin on degenerating rd10 retinas, we subsequently explored the possible underlying mechanism. Specifically, we evaluated the potential impacts of luteolin on apoptosis, oxidative stress, and inflammation using fluorescent staining.

A TUNEL assay was utilized to identify apoptotic photoreceptors (**Figure 6A**). In WT retina, no TUNEL-positive cells were observed (n = 5). Consistent with our prior report (Zhang et al., 2017), numerous TUNEL-positive cells appeared in the ONL of rd10 retinas (2396 ± 311 cells/mm^2, n = 4, P < 0.001, *vs*. WT controls), and treatment with luteolin significantly reduced this number to 478 ± 79 cells/mm^2 (n = 5, P < 0.001 *vs*. PBS; **Figure 6B**). Given that TUNEL-positive cells exclusively represent the apoptotic population (Gavrieli et al., 1992), our results suggest that luteolin attenuated photoreceptor apoptosis in rd10 mice.

To examine whether the aforementioned impact on apoptosis was mediated by modulation of ROS production, we stained retinal sections with the ROS indicator DHE (He et al., 2013). As shown in **Figure 6C**, hardly any DHE was observed in WT retina, but its staining intensity was increased by 1.8 ± 0.2-fold in PBS-treated rd10 retina (P < 0.05), indicating an overt increase in ROS production. Luteolin significantly reduced the increase in DHE fluorescent intensity to 1.2 ± 0.04-fold (P < 0.05, *vs*. PBS-treated group; **Figure 6D**), suggesting that it inhibited ROS production in the rd10 retina.

Luteolin inhibits reactive gliosis in retinas of rd10 mice

ROS regulates gliosis of retinal Müller cells (Hu et al., 2015), and reduced ROS protects Müller cells from gliosis (Tan et al., 2015). Thus, we next investigated whether luteolin inhibits reactive gliosis, as characterized by elevated GFAP expression and reactivity of Iba1-immunolabeled microglial cells.

In accordance with previous literature, Iba1-positive cells were mainly present in the inner plexiform layer and inner retina with branch ramifications (Genové et al., 2014) (**Figure 7A**, left panel). In PBS-treated rd10 mice, microglia were distributed across all layers of the retina at P26, particularly in the outer layers. Many microglia displayed reactive morphologies, i.e. an amoeboid shape with large somas (**Figure 7A**, middle panel). Luteolin treatment reduced numbers of reactive microglia in the outer retina (**Figure 7A**, right panel). To quantify this, we measured the area of Iba-1 positive staining in each section. The Iba-1 positive area of the PBS-treated group increased to 4.8-fold that of WT controls, and luteolin reduced this value to 3.4-fold (P < 0.01, *vs*. PBS group; **Figure 7C**).

Unlike in the WT retina, whereby GFAP staining in Müller cells was limited to their end feet in the nerve fiber layer (**Figure 7B**, left panel), vertically running processes of Müller cells were intensely stained up to their termination in the outer limiting membrane of degenerating rd10 retinas (**Figure 7B**, middle panel). This staining was significantly reduced by luteolin treatment given that the stained processes typically did not cross the ONL (**Figure 7B**, right panel).

To quantify GFAP expression, lengths of GFAP-stained Müller cell processes were measured and their quantities in each section were counted. As shown in **Figure 7D**, the mean length of Müller cell processes was 7.9 ± 0.4 μm (n = 5) in WT controls and significantly increased to 107.6 ± 2.3 μm in PBS-treated rd10 mice (n = 5, P < 0.001; **Figure 7D**). Treatment with luteolin significantly reduced this parameter to 90.0 ± 2.3 μm (n = 5, P < 0.001, *vs*. PBS-treated group). Luteolin further lowered the number of GFAP-positive processes from 37.8 ± 1.2 per image in the PBS-treated rd10 group to 30.6 ± 1.0 per image (P < 0.001; **Figure 7E**). Hence, luteolin alleviated gliosis of Müller cells in rd10 retinas.

Luteolin affects retinal expression of inflammation-related cytokines

As reactive gliosis is a major indicator of inflammation in the retina (Zhang et al., 2017), we next examined retinal expression of inflammation-related molecules by RT-qPCR. These molecules included: (i) pro-inflammatory cytokines interleukin-1 beta (*Il-1β*) and tumor necrosis factor-alpha (*Tnf-α*); (ii) anti-inflammatory cytokines transforming growth factor-beta (*Tgf-β*), arginase 1 (*Arg-1*), interleukin 6 (*Il-6*), interleukin 10 (*Il-10*), and nitric oxide synthase-2 (*Nos-2*); and (iii) chemoattractant cytokines C-C motif chemokine ligand 2 (*Ccl-2*), C-C motif chemokine ligand 3 (*Ccl-3*), and CXC motif chemokine ligand-10 (*Cxcl-10*). As expected, overall expression of the pro-inflammatory and chemoattractant

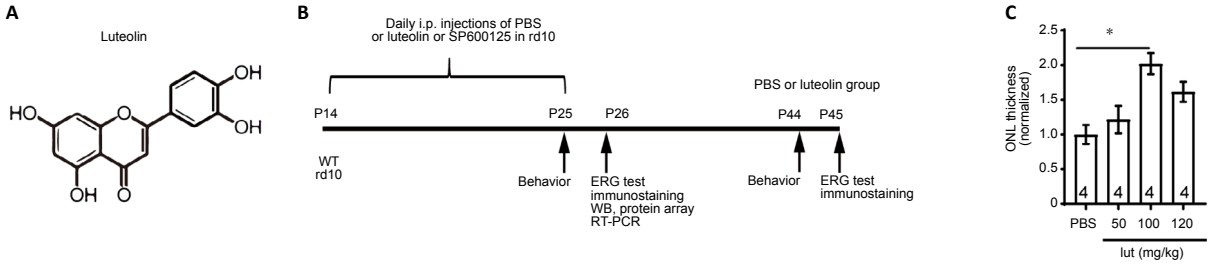

Figure 1 | **Experimental protocol, structure of luteolin, and dose-dependent tests.**
(A) Chemical structure of luteolin. (B) Experimental protocol. In the first set of experiments, rd10 mice at P14 were daily i.p. injected with PBS (n = 28) or luteolin (n = 30) until P25, when assessments started. Age-matched WT mice (n = 25) were utilized as normal controls. Another 13 rd10 mice were kept until P45 to test the long-term effect of luteolin. In the second set of experiments, PBS (n = 4), luteolin (n = 4), or the c-Jun N-terminal kinase inhibitor SP600124 (n = 4) was injected into rd10 mice from P14 to P25. (C) Dose-dependent effects of luteolin (lut) on ONL thickness in rd10 mice at 1 mm away from the center of the optic disk. Values were normalized to PBS-treated controls. Data are expressed as mean ± SEM. *P < 0.05 (one-way analysis of variance followed by Tukey's *post hoc* test). Numbers within bars indicate quantities of mice tested. ERG: Electroretinogram; i.p.: intraperitoneal; ONL: outer nuclear layer; P: postnatal day; PBS: phosphate-buffered saline; RT-PCR: real-time polymerase chain reaction; WB: western blot; WT: wild-type.

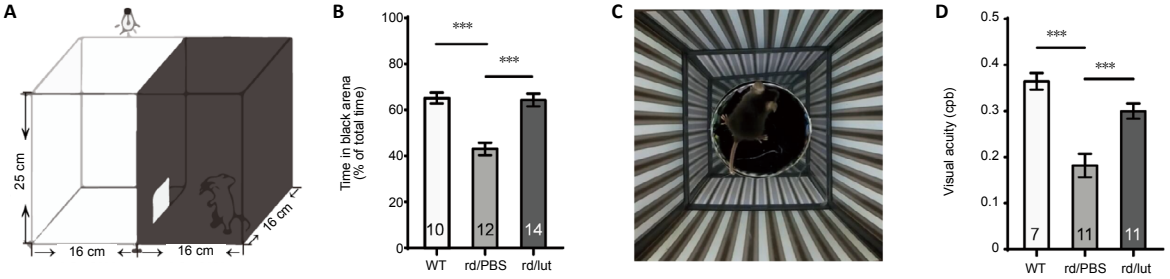

Figure 2 | **Luteolin (lut) improves visual behaviors in rd10 mice.**
(A, C) Illustrations of apparatuses for dark-light transition (A) and optomotor tests (C). (B) Percentages of time during which mice stayed in the dark chamber (relative to the total duration of the test) at P25. (D) Visual acuity (the finest grating at which an animal shows an optomotor reflex) presented in the unit of cycle per degree (cpd). Luteolin treatment increased the duration rd10 mice spent in the darkness and their visual acuity. Data are expressed as mean ± SEM. ***P < 0.001 (one-way analysis of variance followed by Tukey's *post hoc* test). Numbers in bars indicate quantities of mice tested. P: Postnatal day; PBS: phosphate-buffered saline; rd: rd10; WT: wild-type.

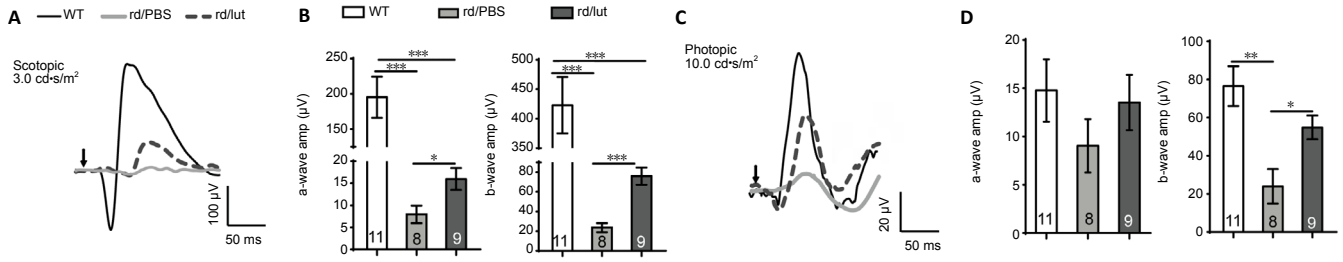

Figure 3 | **Luteolin (lut) improves light responses in the retinas of rd10 mice.**
(A, C) Representative electroretinogram (ERG) traces in response to light flashes under dark adaptation (scotopic 3.0 cd·s/m^2, A) and light adaptation (photopic 10.0 cd·s/m^2, C) from a WT (black lines) or rd10 mouse treated with PBS (gray lines) or luteolin (gray dotted lines) at P26. (B) Peak amplitudes (amp) of the scotopic a- and b-waves. (D) Peak amplitudes (amp) of photopic a- and b-waves. Data are expressed as mean ± SEM. *P < 0.05, **P < 0.01, ***P < 0.001 (Student's t-test). Numbers within bars indicate quantities of mice tested. P: Postnatal day; PBS: phosphate-buffered saline; rd: rd10; WT: wild-type.

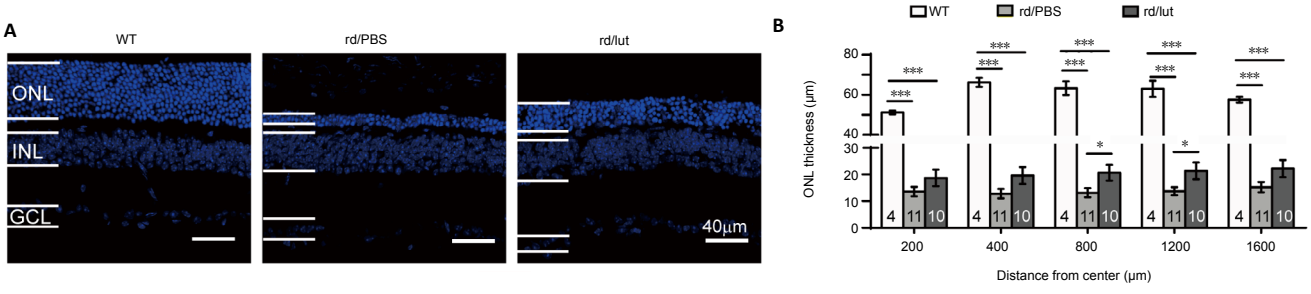

Figure 4 | **Luteolin increases the survival of photoreceptors in rd10 mice.**
(A) Images of DAPI staining of retinal sections. The ONL of retinas of PBS-treated rd10 mice (rd/PBS) was much thinner than that of WT controls, and was partly reversed by luteolin (rd/lut). Scale bars: 40 µm. (B) Quantification of ONL thickness at P26 in each group from center to peripheral regions. Data are expressed as mean ± SEM. *P < 0.05, ***P < 0.001 (one-way analysis of variance followed by Tukey's *post hoc* test). Numbers within bars indicate quantities of mice tested. DAPI: 4′,6-diamidino-2-phenylindole; GCL: ganglion cell layer; INL: inner nuclear layer; ONL: outer nuclear layer; P: postnatal day; PBS: phosphate-buffered saline; WT: wild-type.

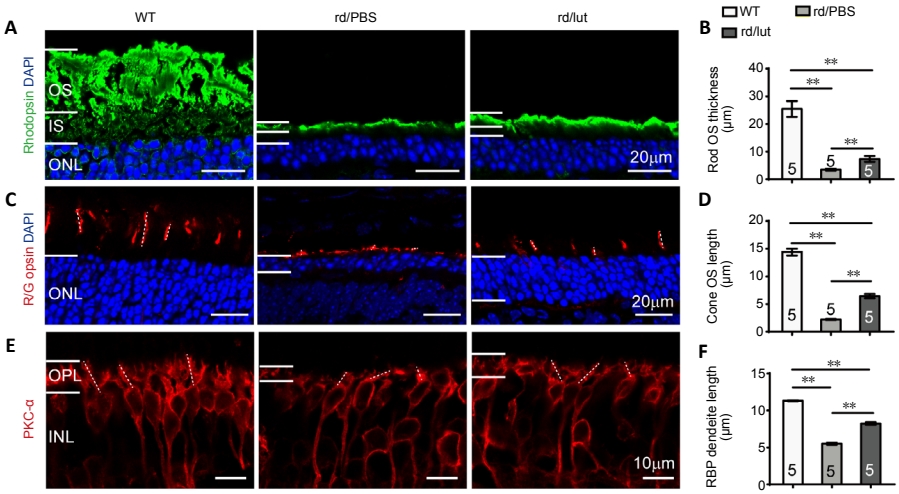

Figure 5 | Luteolin (lut) preserves the morphological structure of photoreceptors and bipolar cells in rd10 mice.
(A, C, E) Images of rhodopsin (Green: Alexa Fluor-488, A), red/green opsin (red: Alexa Fluor-594, C), and PKC-α (red: Alexa Fluor-594, E) which stained the rod outer segment (OS), cone OS and rod bipolar cells, respectively, with DAPI (blue) staining in retinal sections at P26. Dotted lines in C and E illustrate the measured length of several cone OS and RBP dendrites, respectively. Scale bars: 20 μm in A and C, 10 μm in E. (B, D, F) Thickness of rod OS (B), length of cone OS (D), and RBP dendrites (F) in each group. Rod OS, cone OS, and bipolar dendrites were much thinner and shorter in the retinas of rd10 mice compared with WT controls, and luteolin increased these parameters at P26. Data are expressed as mean ± SEM. $^{**}P < 0.01$ (one-way analysis of variance followed by Tukey's *post hoc* test). Numbers within/near bars indicate quantities of mice tested. DAPI: 4′,6-Diamidino-2-phenylindole; INL: inner nuclear layer; IS: inner segment; ONL: outer nuclear layer; OPL: outer plexiform layer; OS: outer segment; P: postnatal day; PBS: phosphate-buffered saline; PKC-α: protein kinase C-α; RBP: rod bipolar cell; rd: rd10; WT: wild-type.

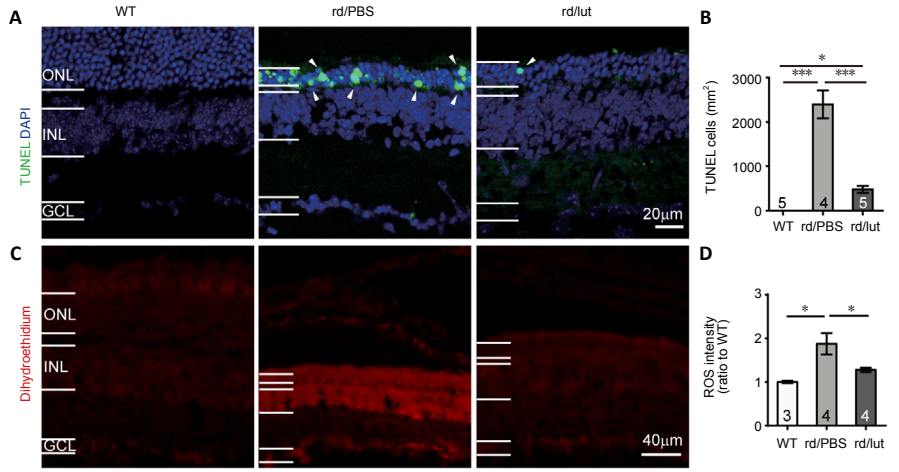

Figure 6 | Luteolin (lut) inhibits apoptosis and oxidative stress in the retinas of rd10 mice.
(A) Images of TUNEL (green) and DAPI (blue) staining of retinal slices at P26 (white arrowheads indicate TUNEL-positive cells). (B) Density of TUNEL-positive cells. In the WT retina, TUNEL-positive (apoptotic) cells were undetected. Apoptotic cells were increased in the retinas of rd10 mice, but were greatly decreased by luteolin. (C) Images of dihydroethidium (DHE, an indicator of ROS production) staining in retinal sections. Scale bars: 20 μm in A, 40 μm in C. (D) Fluorescent intensity of DHE staining across the whole retinal section normalized to the mean of WT controls. ROS levels were elevated in rd10 mice and further reduced by luteolin. Data are expressed as mean ± SEM. $^{*}P < 0.05$, $^{***}P < 0.001$ (one-way analysis of variance followed by Tukey's *post-hoc* test). Numbers within/near bars indicate quantities of mice tested. DAPI: 4′,6-Diamidino-2-phenylindole; GCL: ganglion cell layer; INL: inner nuclear layer; ONL: outer nuclear layer; P: postnatal day; PBS: phosphate-buffered saline; rd: rd10; ROS: reactive oxygen species; TUNEL: terminal deoxynucleotidyl transferase dUTP nick end labeling; WT: wild-type.

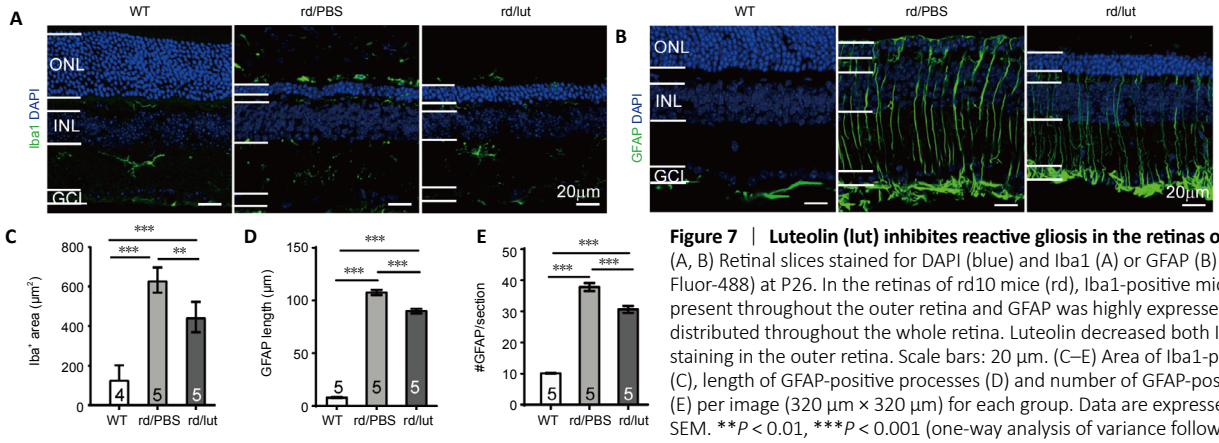

Figure 7 | Luteolin (lut) inhibits reactive gliosis in the retinas of rd10 mice.
(A, B) Retinal slices stained for DAPI (blue) and Iba1 (A) or GFAP (B) (green: Alexa Fluor-488) at P26. In the retinas of rd10 mice (rd), Iba1-positive microglia were present throughout the outer retina and GFAP was highly expressed in Müller cells distributed throughout the whole retina. Luteolin decreased both Iba1 and GFAP staining in the outer retina. Scale bars: 20 μm. (C–E) Area of Iba1-positive staining (C), length of GFAP-positive processes (D) and number of GFAP-positive processes (E) per image (320 μm × 320 μm) for each group. Data are expressed as mean ± SEM. $^{**}P < 0.01$, $^{***}P < 0.001$ (one-way analysis of variance followed by Tukey's *post hoc* test). Numbers within/near bars indicate quantities of mice tested. DAPI: 4′,6-Diamidino-2-phenylindole; GCL: ganglion cell layer; GFAP: glial fibrillary acidic protein; Iba1: ionized calcium-binding adapter molecule 1; INL: inner nuclear layer; ONL: outer nuclear layer; P: postnatal day; PBS: phosphate-buffered saline; WT: wild-type.

cytokines listed above was greatly upregulated in the retinas of rd10 mice (**Figure 8A** and **B**). In contrast, expression of anti-inflammatory cytokines was substantially downregulated (**Figure 8C**). Treatment with luteolin reversed these changes by decreasing mRNA levels of pro-inflammatory and chemoattractant cytokines, while increasing those of anti-inflammatory cytokines. Specifically, compared with the PBS group, decreases of pro-inflammatory *Il-1β* and *Tnf-α* were highly significant ($P < 0.001$), and that of chemoattractants was either highly significant ($P < 0.01$ for *Ccl-2*) or significant ($P < 0.05$ for Ccl-3 and *Cxcl-10*). Notably, *Tgf-β* expression in luteolin-treated retinas was restored to a normal level and highly significant compared with PBS-injected mice ($P < 0.001$).

Luteolin inhibits the JNK pathway in retinas of rd10 mice

The MAPK family reportedly responds to inflammation (Yao et al., 2017). For example, phosphorylation of JNK is closely associated with the overproduction of inflammatory mediators, as well as the occurrence of inflammation (Wang et al., 2020). Here, we used western blotting and protein arrays to identify potential signaling pathways involved in luteolin-mediated protection against retinal degeneration. As shown in **Figure 9A**, there was hardly any change in the p-ERK to ERK ratio in all three conditions. In contrast, although there was no significant difference between the ratio of p-JNK/JNK in WT and rd10 retinas, this ratio was greatly reduced in luteolin-treated mice (**Figure 9B**), suggesting that luteolin may play an inhibitory role in JNK signaling. To further unravel the underlying mechanism, we applied a protein array and screened the expression of targets involved in multiple pathways potentially regulated by luteolin, including AKT, mammalian target of rapamycin (mTOR), adenosine 5′-monophosphate-activated protein kinase (AMPK), phosphatase and tensin homologue deleted on chromosome ten (PTEN), ERK, and p38 mitogen-activated protein kinase (p38MAPK). However, none of these pathways seemed responsible for the neuroprotection elicited by luteolin, as changes in the phosphorylation of key targets following luteolin treatment were insignificant compared with PBS-treated rd10 counterparts (**Figure 9C**).

To substantiate the regulatory role of the JNK pathway in luteolin-elicited neuroprotection, the JNK antagonist SP600125 was injected into rd10 mice using the same protocol described above. As shown in **Figure 10**, injection of luteolin or SP600125 alone significantly increased the ONL thickness compared with their respective solvent controls. These results indicate that in RP mice, inhibiting the JNK pathway contributes to the delay of photoreceptor degeneration.

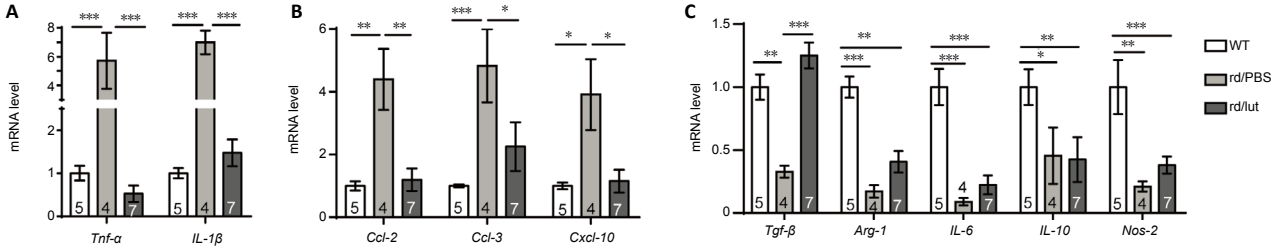

Figure 8 | **Effects of luteolin (lut) on mRNA expression of inflammation-related cytokines in retinas of rd10 mice (rd).**
(A–C) mRNA expression of pro-inflammatory cytokines *Tnf-α* and *Il-1β* (A); chemoattractant cytokines *Ccl-2*, *Ccl-3*, and *Cxcl-10* (B); and anti-inflammatory cytokines *Tgf-β*, *Arg-1*, *Il-6*, *Il-10*, and *Nos-2* (C) in each group at P26, quantified by real-time polymerase chain reaction. Luteolin significantly decreased upregulation of pro-inflammatory and chemoattractant cytokines in the retinas of rd10 mice, and significantly increased *Tgf-β*. Data were normalized to those of WT controls. Data are expressed as mean ± SEM. *$P < 0.05$, **$P < 0.01$, ***$P < 0.001$ (one-way analysis of variance followed by Tukey's *posthoc* test). Numbers within/near bars indicate quantities of mice tested. Arg-1: Arginase 1; Ccl: C-C motif chemokine ligand; Il: interleukin; Nos2: nitric oxide synthase 2; Tgf-β1: transforming growth factor β1; Tnf-α: tumor necrosis factor α; P: postnatal day; PBS: phosphate-buffered saline; WT: wild-type.

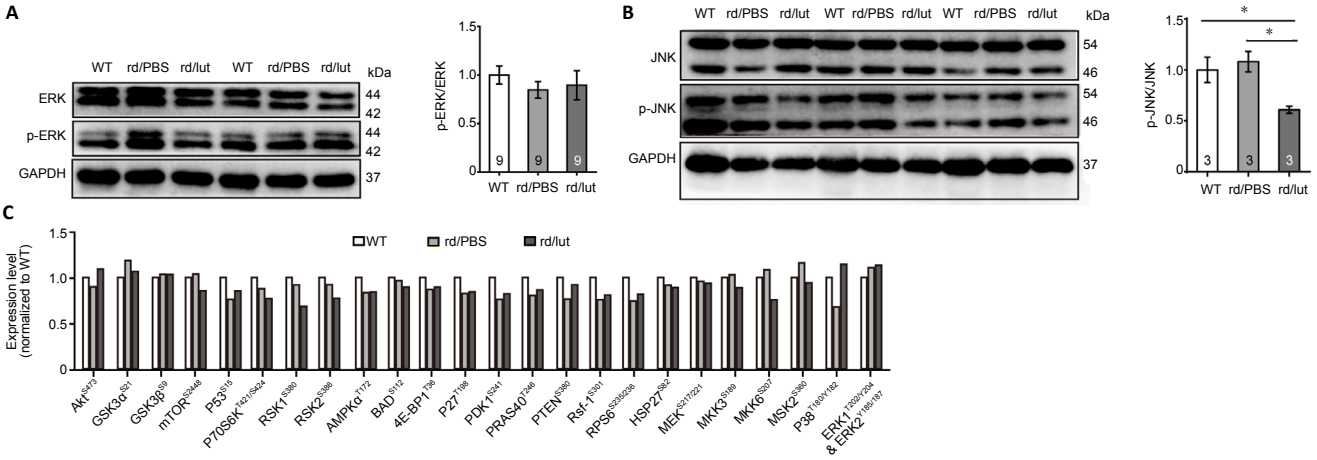

Figure 9 | **Luteolin inhibited (lut) the JNK pathway in the retinas of rd10 mice (rd).**
(A) Images of western blots (left panel) showing expression of ERK and p-ERK, with GAPDH as a loading control, at P26. Ratios of p-ERK/ERK for each sample are shown on the right. (B) Western blots of JNK and p-JNK (left panel) and ratios of p-JNK to JNK for each sample (right panel). Data are expressed as mean ± SEM. Data were calculated from at least three independent experiments. *$P < 0.05$ (one-way analysis of variance followed by Tukey's *post hoc* test). Numbers within bars indicate quantities of mice tested. (C) Changes in expression levels of the phosphorylated forms of key signaling molecules after specified treatments by protein array assays. Data were averaged from two independent repeats: the first test used protein samples of both retinas from five WT, three PBS-treated, and three luteolin-treated mice; while the second used five WT, four PBS-treated, and three luteolin-treated mice. 4E-BP1: Eukaryotic translation initiation factor 4E-binding protein 1; Akt: protein kinase B; AMPKα: adenosine 5′-monophosphate-activated protein kinase α; BAD: Bcl-xL/Bcl-2-associated death promoter; ERK: extracellular-signal-regulated kinase; GAPDH: glyceraldehyde 3-phosphate dehydrogenase; GSK: glycogen synthase kinase; HSP27: heat shock protein 27; JNK: c-Jun N-terminal kinase; MEK: mitogen-activated protein kinase-extracellular-signal-regulated kinase kinase; MKK: mitogen-activated protein kinase kinase; MSK: mitogen-and-stress-activated protein kinase; mTOR: mammalian target of rapamycin; P: postnatal day; P70S6K: 70-kDa ribosomal protein S6 kinase; PBS: phosphate-buffered saline; PDK1: phosphoinositide-dependent protein kinase 1; p-ERK: phosphorylated extracellular-signal-regulated kinase; p-JNK: phosphorylated JNK; PRAS40: proline-rich Akt substrate of 40 KD; PTEN: phosphatase and tensin homologue deleted on chromosome ten; Raf-1: rapidly accelerated fibrosarcoma-1; RPS6: ribosomal protein S6; RSK: ribosomal S6 kinase; WT: wild-type.

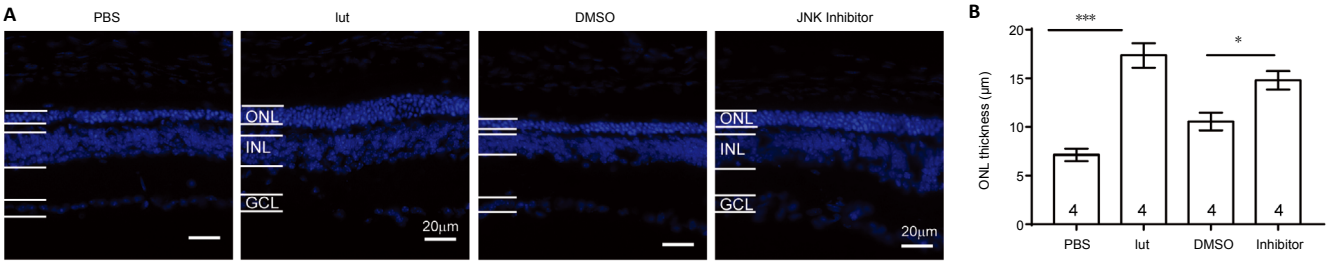

Figure 10 | **The JNK inhibitor SP600125 preserved the retinal morphology of rd10 mice (rd) .**
(A) Representative images of DAPI-stained retinal slices from rd10 mice treated with PBS, luteolin (lut), DMSO, or the JNK inhibitor SP600125 at P26. Scale bars: 20 μm. (B) ONL thickness in rd10 retinal slices at approximately 1 mm from the center of the optic disk. Treatment with luteolin or the JNK inhibitor increased ONL thickness compared with solvent controls. Data are expressed as mean ± SEM. **P* < 0.05, ****P* < 0.001 (Student's *t*-test). Numbers within bars indicate quantities of mice tested. DAPI: 4′,6-Diamidino-2-phenylindole; DMSO: dimethyl sulfoxide; JNK: c-Jun N-terminal kinase; GCL: ganglion cell layer; INL: inner nuclear layer; ONL: outer nuclear layer; P: postnatal day; PBS: phosphate-buffered saline.

Discussion

In the current study, we determined the effects of luteolin on the retina of Pde6b^{rd10} (rd10) mutant mice. Here, we demonstrated for the first time by both functional and morphological tests that luteolin slows down photoreceptor degeneration in rd10 mice. Our study further elucidated the potential mechanisms accounting for its action: luteolin inhibits JNK signaling and, hence, may affect several downstream processes such as attenuating apoptosis and ROS production, thus alleviating reactive gliosis in Müller cells and microglia. Furthermore, luteolin downregulated pro-inflammatory cytokine expression while increasing that of anti-inflammatory cytokines.

Protection of rd10 retinas by luteolin

We first demonstrated that luteolin administered by i.p. injection could penetrate the retina-blood barrier and reach the retina at a concentration proven to effectively protect cultured retinal ganglion cells against oxidative stress injury (Maher and Hanneken, 2005). These results are in line with a previous study reporting the capacity of luteolin to cross the blood-brain barrier (You et al., 2019). Our results set a basis for future application of luteolin to ophthalmic disorders. Of note, although a single injection led to an immediate increase in the retina, the turnover seemed fast. Hence, a protocol involving repeated administration is required and could be further optimized in the future.

With an appropriate dose of 100 mg/kg body weight, our results showed that luteolin treatment almost fully restored the visual behaviors of rd10 mice to that of WT controls under both scotopic and photopic conditions. Consistent with the observed functional amelioration, our morphological data indicated significant preservation of cone and rod outer segments following luteolin treatment (44% and 19% of WT, respectively). It is worth noting that our results were consistent with previous findings indicating that luteolin treatment almost completely reverses optomotor dysfunction in rd10 mice, despite the partial recovery of scotopic vision and modest restoration of ONL thickness (Zhang et al., 2017). Considering that cones contribute much more to optokinetic responses than rods (Schroeder et al., 2018), whereas rods are the dominant photoreceptors in scotopic vision (Lamb, 2016), we concluded that cones may be a more appropriate target for luteolin treatment and even a small histological improvement is worth pursuing, as it has a greater consequence in enhancing function.

While the observed short-term protection was impressive, the long-term effect was negligible as tested by photoreceptor survival, ERG, and optomotor response (**Additional Figure 1**). These results may be explained by our choice to provide treatment only until P25, suggesting that the beneficial effects of luteolin may be associated with the duration of its treatment. A less likely explanation is that the therapeutic effects of luteolin on retinal degeneration are time-sensitive (i.e. luteolin is more effective at the early stage of RP). It is also possible that luteolin targets only certain pathological pathways activated during RP, and therefore its protection is incomplete. Nonetheless, the short-term amelioration of RP-elicited morphological and functional impairments in vision demonstrated by the current study shed light on a novel strategy for retinal protection by the flavonoid luteolin.

Possible mechanisms mediating the neuroprotection elicited by luteolin

The neuroprotective role of luteolin both *in vivo* and *in vitro* has been documented in experimental models of several central nervous system disorders, including traumatic brain injury (Wang et al., 2020), epilepsy (Waetzig and Herdegen, 2004), ischemia (Repici and Borsello, 2006), Alzheimer's disease (Choi and Lee, 2010), and Parkinson's disease (Patil et al., 2014). However, the underlying mechanism for its neuroprotective effect is still debated. Numerous molecules are reportedly dynamically modulated by luteolin. To name a few, nuclear factor kappa-B (NF-κB), malondialdehyde, myc promoter-binding protein, GFAP, matrix metalloprotein-9 (MMP-9), tissue inhibitor of metalloproteinases, caspase-3, Toll-like receptors 4 and 5, phosphorylated ERK1/2 or AKT, nitric oxide, Bax, and P53-targeting genes can all be reduced by luteolin. Likewise, activities of enzymes such as chymase and tryptase are also reduced following luteolin administration. In addition, luteolin is able to suppress the activation of certain immune cells, such as microglia, and can upregulate MMP2, neurotrophic factors (brain-derived neurotrophic factor and glial cell line-derived neurotrophic factor), anti-oxidative enzymes (superoxide dismutase and glutathione peroxidase), mTOR, nuclear factor E2-related factor, B-cell lymphoma 2, heme oxygenase-1, beclin 1, microtubule-associated protein light chain 3 II, and interferon-gamma (Liao et al., 2018). Taken together, these findings imply that luteolin-elicited biological alterations, albeit multi-faceted, are likely disease-specific. Accordingly, we explored the potential mechanisms underlying its neuroprotection in retinal degeneration by referring to previous studies on other central nervous system disorders.

Flavonoids are known for their capacity to scavenge ROS, subsequently mitigating oxidative stress. Following this hint, we measured ROS levels in degenerating rd10 retinas, which revealed that luteolin significantly lowered this pathogenic factor. Furthermore, treatment with luteolin cytologically inhibited reactive gliosis of both Müller cells and microglia, which are both putatively regarded to play important roles in the progression of RP, whereby neuroinflammation may be a key issue resulting in photoreceptor degeneration. Hence, we next examined the influence of luteolin on transcription levels of three subsets of immune-related molecules: pro-inflammatory cytokines *Tnf-α* and *Il-1β*, which clearly

aggravate inflammation, produce fever, and cause tissue destruction when administered to humans (Dinarello, 2000); anti-inflammatory cytokines *Tgf-β*, *Arg-1*, *Il-6*, *Il-10*, and *Nos-2*; and chemoattractant cytokines *Ccl-2*, *Ccl-3*, and *Cxcl-10*, which are associated with the development of neurodegenerative diseases such as Parkinson's disease and Alzheimer's disease (Ramesh et al., 2013). In line with previous reports, the retina of rd10 mice exhibited overt neuroinflammation, as evidenced by significantly increased expression of pro-inflammatory and chemoattractant cytokines, and reduced expression of anti-inflammatory cytokines. For targets *Tnf-α*, *Il-1β*, *Tgf-β*, *Ccl-2*, *Ccl-3*, and *Cxcl-10*, luteolin-triggered reversibility in mRNA expression reached statistical significance, supporting the notion that suppressing excessive inflammatory responses assists in counteracting retinal degeneration in rd10 mice. Notably, the restoration of anti-inflammatory capacity by increased expression of other targets (including *Arg-1*, *Il-10*, and *Nos-2*) was marginal, which may account for the incomplete recovery in luteolin-treated rd10 mice. It is worth mentioning that *Il-6* is a pleiotropic factor that can elicit both regenerative and anti-inflammatory changes, or aggravate inflammation, thus exerting a double-edged sword effect on immune responses. Many studies have highlighted its crucial anti-inflammatory role in regulating immune cells. For instance, *Il-6* reportedly mediates immunosuppression in dendritic cells by upregulating expression of the anti-inflammatory cytokine *Il-10*, which reduces the binding activity of NF-κB and suppresses transcription of CCR7 (Hegde et al., 2004). Likewise, *Il-6* inhibits the inflammatory response in bacterial meningitis by reducing leukocyte infiltration (Paul et al., 2003). Interestingly, although *Il-6* reportedly had adverse impacts on the retina (Balasubramaniam et al., 2009; Robinson et al., 2020), there are also studies confirming its retinal neuroprotective property. For example, treatment with *Il-6* promoted the survival of retinal ganglion cells by upregulating brain-derived neurotrophic factor via activation of adenosine receptors A1R and A2aR (Mendonça Torres and de Araujo, 2001; Perígolo-Vicente et al., 2013, 2014). Likewise, intravitreal injection of *Il-6* increased the endogenous level of ciliary neurotrophic factor to protect photoreceptors against retinal degeneration (Heo et al., 2018). Taken together, *Il-6* may play differential roles in the retina, whose effects may be cell- and disease-specific, and influenced by the adjacent milieu. In the current study, *Il-6* was more likely to attenuate overall inflammation, given its similar expression pattern compared with other anti-inflammatory cytokines in the retina. The increase of *Il-6* levels was insignificant in luteolin-treated rd10 retinas, which we speculated might be somehow associated with the observed incomplete restoration of visual function; thus, the immunoregulatory role of *Il-6* observed during this process warrants further investigation.

In terms of potential signaling pathways enabling the aforementioned cellular and immune responses, we employed phosphorylation protein array screening concurrently with semi-quantitative immunoblotting. The results showed that with the exception of a significant reduction in the ratio of p-JNK to total JNK, dynamic changes of other numerous targets were not evident. JNK, a serine-threonine protein kinase belonging to the MAPK family, regulates a variety of cellular activities such as proliferation, differentiation, apoptosis, inflammation, and so forth. Of note, phosphorylation of JNK is closely related to the overproduction of inflammatory mediators and occurrence of inflammation (Wang et al., 2020). As a result, blocking of the JNK signaling pathway has been raised as a potential therapeutic strategy to prevent neurodegenerative and neuroinflammatory diseases (Repici and Borsello, 2006). Results of the current research support this conjecture by showing that luteolin treatment of rd10 mice reduced phosphorylated JNK and directly inhibited the JNK pathway to protect photoreceptors from degeneration. Interestingly, while some previous literature reported that luteolin suppresses phosphorylation of JNK (Choi and Lee, 2010; Kao et al., 2011; Wu et al., 2020), others show the opposite result (Liao et al., 2018; You et al., 2019). The discrepancy may arise from the fact that luteolin-induced activation and inhibition of the JNK pathway is concentration-dependent (Kimata et al., 2000), which consequently indicates that the dosage of luteolin is critical and, perhaps, requires individualization. Notably, JNK inhibitors including SP600125, UTI, LXA4, and Celastrol have been discovered to potently downregulate levels of pro-inflammatory cytokines and chemokines, while upregulating those of anti-inflammatory ones (Miao et al., 2015; An et al., 2017; Li et al., 2018; Zhang et al., 2020). This is consistent with our results and further emphasizes the role of the JNK pathway in mediating luteolin-conferred protection of photoreceptors. Despite the fact that other pathways such as Raf1-MEK-1-Erk, p38MAPK, and mTOR also reportedly participate in the regulation of neuroinflammation by luteolin (Wu et al., 2013; Yang et al., 2018; Ye et al., 2019), the pilot data from our protein array screening did not support this possibility.

There are several limitations of the current study that need to be considered. For instance, luteolin-exerted protection of photoreceptors is suggested to be mediated through the JNK signaling pathway based on results showing that luteolin lowered phosphorylation of JNK and the JNK inhibitor SP600125 recapitulated the effect of luteolin on retinal morphology. Nevertheless, application of a JNK activator (e.g. anisomycin) following luteolin treatment should be performed to examine whether such protection can be diminished, as this would further strengthen our conclusion. Likewise, retinal samples used for molecular assays were obtained at the end point. Therefore, potential dynamic changes of experimental indices, such as mRNA levels of inflammation-related cytokines and activation of various signaling pathways, remain unknown. Accordingly, assessments with more time points are preferred for future investigations. Additionally, while luteolin seems promising for RP treatment in the current situation, it remains unclear whether these findings allow for direct clinical translation, particularly considering the incomplete and transient protection elicited by luteolin in rd10 mice, which exhibit much faster degeneration than human subjects. Hence, well-designed clinical trials with optimization of luteolin administration in RP patients are needed.

In summary, our current study demonstrated that administration of luteolin can effectively delay the progressive impairments of retinal morphology and visual functions in rd10 mice. These therapeutic effects potentially depend on reducing ROS and photoreceptor apoptosis, and inhibiting reactive gliosis of Müller cells and microglial activation. The observed decrease in phosphorylation of JNK and subsequent correction of exaggerated neuroinflammation could be the underlying molecular mechanism. As an herbal extract, luteolin exhibits comprehensive beneficial effects and is therefore promising for treating RP and other retinal disorders involving neurodegeneration and neuroinflammation.

Acknowledgments: *The authors thank Noga Vardi for helpful suggestions and proofreading this manuscript, and Mengrong Zhang and Renzhi Li for technical assistance.*

Author contributions: *Study design: AL, YX; experiment performance: XBL, FL, YYL, GY, HJZ; data analysis: XBL, FL, GY, AL, YX; manuscript preparation: AL, YX; manuscript editing and review: XSM, ZJZ, KFS, AL, YX. All authors approved the final version of the paper.*

Conflicts of interest: *The authors indicated no potential conflicts of interest.*

Financial support: *The work was supported by the National Natural Science Foundation of China, Nos. 81470656 (to YX), 82071372 (to AL), 82074169 (to XSM); Guangdong Grant 'Key Technologies for Treatment of Brain Disorders', China, No. 2018B030332001 (to YX); Ningxia Key Research and Development Program Grant (Yinchuan, Ningxia Hui Autonomous Region, China) (to KFS); Program of Introducing Talents of*

Discipline to Universities, China, No. B14036 (to YX, AL, KFS); Outstanding Scholar Program of Bioland Laboratory (Guangzhou Regenerative Medicine and Health Guangdong Laboratory), No. 2018GZR110102002 (to KFS, AL); and Science and Technology Program of Guangzhou, No. 202007030012 (to KFS and AL). The funders had no roles in the study design, conduction of experiment, data collection and analysis, decision to publish, or preparation of the manuscript.
Institutional review board statement: *This study was approved by the Qualified Ethics Committee of Jinan University, China (approval No. IACUC-20181217-02) on December 17, 2018.*

Data sharing statement: *Datasets analyzed during the current study are available from the corresponding author on reasonable request.*
Plagiarism check: *Checked twice by iThenticate.*
Peer review: *Externally peer reviewed.*

Open peer reviewer: *Rithwick Rajagopal, Washington University, USA.*
Additional files:
Additional Figure 1: *Long-term effects of luteolin in rd10 mice.*
Additional Figure 2: *Effects of luteolin on scotopic ERG responses at various flash intensities in rd10 mice.*

References

An SY, Youn GS, Kim H, Choi SY, Park J (2017) Celastrol suppresses expression of adhesion molecules and chemokines by inhibiting JNK-STAT1/NF-κB activation in poly(I:C)-stimulated astrocytes. BMB Rep 50:25-30.

Azadi S, Johnson LE, Paquet-Durand F, Perez MT, Zhang Y, Ekström PA, van Veen T (2007) CNTF+BDNF treatment and neuroprotective pathways in the rd1 mouse retina. Brain Res 1129:116-129.

Balasubramaniam B, Carter DA, Mayer EJ, Dick AD (2009) Microglia derived IL-6 suppresses neurosphere generation from adult human retinal cell suspensions. Exp Eye Res 89:757-766.

Barhoum R, Martínez-Navarrete G, Corrochano S, Germain F, Fernandez-Sanchez L, de la Rosa EJ, de la Villa P, Cuenca N (2008) Functional and structural modifications during retinal degeneration in the rd10 mouse. Neuroscience 155:698-713.

Chang B, Hawes NL, Pardue MT, German AM, Hurd RE, Davisson MT, Nusinowitz S, Rengarajan K, Boyd AP, Sidney SS, Phillips MJ, Stewart RE, Chaudhury R, Nickerson JM, Heckenlively JR, Boatright JH (2007) Two mouse retinal degenerations caused by missense mutations in the beta-subunit of rod cGMP phosphodiesterase gene. Vision Res 47:624-633.

Chen CY, Peng WH, Tsai KD, Hsu SL (2007) Luteolin suppresses inflammation-associated gene expression by blocking NF-kappaB and AP-1 activation pathway in mouse alveolar macrophages. Life Sci 81:1602-1614.

Choi EM, Lee YS (2010) Luteolin suppresses IL-1beta-induced cytokines and MMPs production via p38 MAPK, JNK, NF-kappaB and AP-1 activation in human synovial sarcoma cell line, SW982. Food Chem Toxicol 48:2607-2611.

Dinarello CA (2000) Proinflammatory cytokines. Chest 118:503-508.

Dirscherl K, Karlstetter M, Ebert S, Kraus D, Hlawatsch J, Walczak Y, Moehle C, Fuchshofer R, Langmann T (2010) Luteolin triggers global changes in the microglial transcriptome leading to a unique anti-inflammatory and neuroprotective phenotype. J Neuroinflammation 7:3.

Gargini C, Terzibasi E, Mazzoni F, Strettoi E (2007) Retinal organization in the retinal degeneration 10 (rd10) mutant mouse: a morphological and ERG study. J Comp Neurol 500:222-238.

Gavrieli Y, Sherman Y, Ben-Sasson SA (1992) Identification of programmed cell death in situ via specific labeling of nuclear DNA fragmentation. J Cell Biol 119:493-501.

Genové G, Mollick T, Johansson K (2014) Photoreceptor degeneration, structural remodeling and glial activation: a morphological study on a genetic mouse model for pericyte deficiency. Neuroscience 279:269-284.

Hanneken A, Lin FF, Johnson J, Maher P (2006) Flavonoids protect human retinal pigment epithelial cells from oxidative-stress-induced death. Invest Ophthalmol Vis Sci 47:3164-3177.

Hartong DT, Berson EL, Dryja TP (2006) Retinitis pigmentosa. Lancet 368:1795-1809.

He M, Pan H, Xiao C, Pu M (2013) Roles for redox signaling by NADPH oxidase in hyperglycemia-induced heme oxygenase-1 expression in the diabetic retina. Invest Ophthalmol Vis Sci 54:4092-4101.

Head KA (1999) Natural therapies for ocular disorders, part one: diseases of the retina. Altern Med Rev 4:342-359.

Hegde S, Pahne J, Smola-Hess S (2004) Novel immunosuppressive properties of interleukin-6 in dendritic cells: inhibition of NF-kappaB binding activity and CCR7 expression. FASEB J 18:1439-1441.

Hendriks JJ, Alblas J, van der Pol SM, van Tol EA, Dijkstra CD, de Vries HE (2004) Flavonoids influence monocytic GTPase activity and are protective in experimental allergic encephalitis. J Exp Med 200:1667-1672.

Heo JH, Yoon JA, Ahn EK, Kim H, Urm SH, Oak CO, Yu BC, Lee SJ (2018) Intraperitoneal administration of adipose tissue-derived stem cells for the rescue of retinal degeneration in a mouse model via indigenous CNTF up-regulation by IL-6. J Tissue Eng Regen Med 12:e1370-e1382.

Herrera-Hernández MG, Ramon E, Lupala CS, Tena-Campos M, Pérez JJ, Garriga P (2017) Flavonoid allosteric modulation of mutated visual rhodopsin associated with retinitis pigmentosa. Sci Rep 7:11167.

Hu Q, Huang C, Wang Y, Wu R (2015) Expression of leukemia inhibitory factor in the rat retina following acute ocular hypertension. Mol Med Rep 12:6577-6583.

Hytti M, Piippo N, Korhonen E, Honkakoski P, Kaarniranta K, Kauppinen A (2015) Fisetin and luteolin protect human retinal pigment epithelial cells from oxidative stress-induced cell death and regulate inflammation. Sci Rep 5:17645.

Jiang K, Wright KL, Zhu P, Szego MJ, Bramall AN, Hauswirth WW, Li Q, Egan SE, McInnes RR (2014) STAT3 promotes survival of mutant photoreceptors in inherited photoreceptor degeneration models. Proc Natl Acad Sci U S A 111:E5716-5723.

Kao TK, Ou YC, Lin SY, Pan HC, Song PJ, Raung SL, Lai CY, Liao SL, Lu HC, Chen CJ (2011) Luteolin inhibits cytokine expression in endotoxin/cytokine-stimulated microglia. J Nutr Biochem 22:612-624.

Kimata M, Shichijo M, Miura T, Serizawa I, Inagaki N, Nagai H (2000) Effects of luteolin, quercetin and baicalein on immunoglobulin E-mediated mediator release from human cultured mast cells. Clin Exp Allergy 30:501-508.

Lamb TD (2016) Why rods and cones? Eye (Lond) 30:179-185.

Li ST, Dai Q, Zhang SX, Liu YJ, Yu QQ, Tan F, Lu SH, Wang Q, Chen JW, Huang HQ, Liu PQ, Li M (2018) Ulinastatin attenuates LPS-induced inflammation in mouse macrophage RAW264.7 cells by inhibiting the JNK/NF-κB signaling pathway and activating the PI3K/Akt/Nrf2 pathway. Acta Pharmacol Sin 39:1294-1304.

Liao Y, Xu Y, Cao M, Huan Y, Zhu L, Jiang Y, Shen W, Zhu G (2018) Luteolin induces apoptosis and autophagy in mouse macrophage ANA-1 cells via the Bcl-2 pathway. J Immunol Res 2018:4623919.

Liu F, Zhang J, Xiang Z, Xu D, So KF, Vardi N, Xu Y (2018) Lycium Barbarum polysaccharides protect retina in rd1 mice during photoreceptor degeneration. Invest Ophthalmol Vis Sci 59:597-611.

Liu Y, Gou LS, Tian X, Fu XB, Ling X, Sun LY, Lan N, Li S, Yin XX (2013) Protective effects of luteolin on cognitive impairments induced by psychological stress in mice. Exp Biol Med (Maywood) 238:418-425.

Maher P, Hanneken A (2005) Flavonoids protect retinal ganglion cells from oxidative stress-induced death. Invest Ophthalmol Vis Sci 46:4796-4803.

Mendonça Torres PM, de Araujo EG (2001) Interleukin-6 increases the survival of retinal ganglion cells in vitro. J Neuroimmunol 117:43-50.

Miao GS, Liu ZH, Wei SX, Luo JG, Fu ZJ, Sun T (2015) Lipoxin A4 attenuates radicular pain possibly by inhibiting spinal ERK, JNK and NF-κB/p65 and cytokine signals, but not p38, in a rat model of non-compressive lumbar disc herniation. Neuroscience 300:10-18.

Park SW, Cho CS, Jun HO, Ryu NH, Kim JH, Yu YS, Kim JS, Kim JH (2012) Anti-angiogenic effect of luteolin on retinal neovascularization via blockade of reactive oxygen species production. Invest Ophthalmol Vis Sci 53:7718-7726.

Patil SP, Jain PD, Sancheti JS, Ghumatkar PJ, Tambe R, Sathaye S (2014) Neuroprotective and neurotrophic effects of Apigenin and Luteolin in MPTP induced parkinsonism in mice. Neuropharmacology 86:192-202.

Paul R, Koedel U, Winkler F, Kieseier BC, Fontana A, Kopf M, Hartung HP, Pfister HW (2003) Lack of IL-6 augments inflammatory response but decreases vascular permeability in bacterial meningitis. Brain 126:1873-1882.

Pawlowska E, Szczepanska J, Koskela A, Kaarniranta K, Blasiak J (2019) Dietary polyphenols in age-related macular degeneration: protection against oxidative stress and beyond. Oxid Med Cell Longev 2019:9682318.

Perígolo-Vicente R, Ritt K, Pereira MR, Torres PM, Paes-de-Carvalho R, Giestal-de-Araujo E (2013) IL-6 treatment increases the survival of retinal ganglion cells in vitro: the role of adenosine A1 receptor. Biochem Biophys Res Commun 430:512-518.

Perígolo-Vicente R, Ritt K, Gonçalves-de-Albuquerque CF, Castro-Faria-Neto HC, Paes-de-Carvalho R, Giestal-de-Araujo E (2014) IL-6, A1 and A2aR: a crosstalk that modulates BDNF and induces neuroprotection. Biochem Biophys Res Commun 449:477-482.

Prusky GT, Alam NM, Beekman S, Douglas RM (2004) Rapid quantification of adult and developing mouse spatial vision using a virtual optomotor system. Invest Ophthalmol Vis Sci 45:4611-4616.

Ramesh G, MacLean AG, Philipp MT (2013) Cytokines and chemokines at the crossroads of neuroinflammation, neurodegeneration, and neuropathic pain. Mediators Inflamm 2013:480739.

Repici M, Borsello T (2006) JNK pathway as therapeutic target to prevent degeneration in the central nervous system. Adv Exp Med Biol 588:145-155.

Robinson R, Youngblood H, Iyer H, Bloom J, Lee TJ, Chang L, Lukowski Z, Zhi W, Sharma A, Sharma S (2020) Diabetes induced alterations in murine vitreous proteome are mitigated by IL-6 trans-signaling inhibition. Invest Ophthalmol Vis Sci 61:2.

Rossino MG, Casini G (2019) Nutraceuticals for the treatment of diabetic retinopathy. Nutrients 11:771.

Schroeder MM, Harrison KR, Jaeckel ER, Berger HN, Zhao X, Flannery MP, St Pierre EC, Pateqi N, Jachimska A, Chervenak AP, Wong KY (2018) The roles of rods, cones, and melanopsin in photoresponses of M4 intrinsically photosensitive retinal ganglion cells (ipRGCs) and optokinetic visual behavior. Front Cell Neurosci 12:203.

Shen H, Wu N, Wang Y, Han X, Zheng Q, Cai X, Zhang H, Zhao M (2017) JNK inhibitor SP600125 attenuates paraquat-induced acute lung injury: an in vivo and in vitro study. Inflammation 40:1319-1330.

Sun X, Shao H, Xiang K, Yan Y, Yu X, Li D, Wu W, Zhou L, So KF, Ren Y, Ramakrishna S, Li A, He L (2017) Poly(dopamine)-modified carbon nanotube multilayered film and its effects on macrophages. Carbon 113:176-191.

Tan SM, Deliyanti D, Figgett WA, Talia DM, de Haan JB, Wilkinson-Berka JL (2015) Ebselen by modulating oxidative stress improves hypoxia-induced macroglial Müller cell and vascular injury in the retina. Exp Eye Res 136:1-8.

Trifunović D, Arango-Gonzalez B, Comitato A, Barth M, Del Amo EM, Kulkarni M, Sahaboglu A, Hauck SM, Urtti A, Arsenijevic Y, Ueffing M, Marigo V, Paquet-Durand F (2016) HDAC inhibition in the cpfl1 mouse protects degenerating cone photoreceptors in vivo. Hum Mol Genet 25:4462-4472.

Waetzig V, Herdegen T (2004) Neurodegenerative and physiological actions of c-Jun N-terminal kinases in the mammalian brain. Neurosci Lett 361:64-67.

Wang K, Xiao J, Peng B, Xing F, So KF, Tipoe GL, Lin B (2014) Retinal structure and function preservation by polysaccharides of wolfberry in a mouse model of retinal degeneration. Sci Rep 4:7601.

Wang YL, Zheng J, Zhang XF, Zhang Y (2020) Attenuation of paraquat-induced inflammation by inhibitors of phosphorylation of mitogen-activated protein kinases in BV(2) microglial cells. J Neurol Sci 410:116679.

Williams RJ, Spencer JP, Rice-Evans C (2004) Flavonoids: antioxidants or signalling molecules? Free Radic Biol Med 36:838-849.

Wu S, Wang HQ, Guo TT, Li YH (2020) Luteolin inhibits CVB3 replication through inhibiting inflammation. J Asian Nat Prod Res 22:762-773.

Wu W, Li D, Zong Y, Zhu H, Pan D, Xu T, Wang T, Wang T (2013) Luteolin inhibits inflammatory responses via p38/MK2/TTP-mediated mRNA stability. Molecules 18:8083-8094.

Xiang Z, Bao Y, Zhang J, Liu C, Xu D, Liu F, Chen H, He L, Ramakrishna S, Zhang Z, Vardi N, Xu Y (2018) Inhibition of non-NMDA ionotropic glutamate receptors delays the retinal degeneration in rd10 mouse. Neuropharmacology 139:137-149.

Yang S, Luo X, Xiong G, So KF, Yang H, Xu Y (2015) The electroretinogram of Mongolian gerbil (Meriones unguiculatus): comparison to mouse. Neurosci Lett 589:7-12.

Yang SC, Chen PJ, Chang SH, Weng YT, Chang FR, Chang KY, Chen CY, Kao TI, Hwang TL (2018) Luteolin attenuates neutrophilic oxidative stress and inflammatory arthritis by inhibiting Raf1 activity. Biochem Pharmacol 154:384-396.

Yao B, Wang S, Xiao P, Wang Q, Hea Y, Zhang Y (2017) MAPK signaling pathways in eye wounds: Multifunction and cooperation. Exp Cell Res 359:10-16.

Ye S, Liu H, Chen Y, Qiu F, Liang CL, Zhang Q, Huang H, Wang S, Zhang ZD, Lu W, Dai Z (2019) A novel immunosuppressant, luteolin, modulates alloimmunity and suppresses murine allograft rejection. J Immunol 203:3436-3446.

You Y, Wang R, Shao N, Zhi F, Yang Y (2019) Luteolin suppresses tumor proliferation through inducing apoptosis and autophagy via MAPK activation in glioma. Onco Targets Ther 12:2383-2396.

Zhang J, Xu D, Ouyang H, Hu S, Li A, Luo H, Xu Y (2017) Neuroprotective effects of methyl 3,4 dihydroxybenzoate in a mouse model of retinitis pigmentosa. Exp Eye Res 162:86-96.

Zhang J, Lin W, Tang M, Zhao Y, Zhang K, Wang X, Li Y (2020) Inhibition of JNK ameliorates depressive-like behaviors and reduces the activation of pro-inflammatory cytokines and the phosphorylation of glucocorticoid receptors at serine 246 induced by neuroinflammation. Psychoneuroendocrinology 113:104580.

Ziyan L, Yongmei Z, Nan Z, Ning T, Baolin L (2007) Evaluation of the anti-inflammatory activity of luteolin in experimental animal models. Planta Med 73:221-226.

P-Reviewer: Rajagopal R; C-Editor: Zhao M; S-Editors: Yu J, Li CH; L-Editors: Deusen AV, Yu J, Song CP; T-Editor: Jia Y

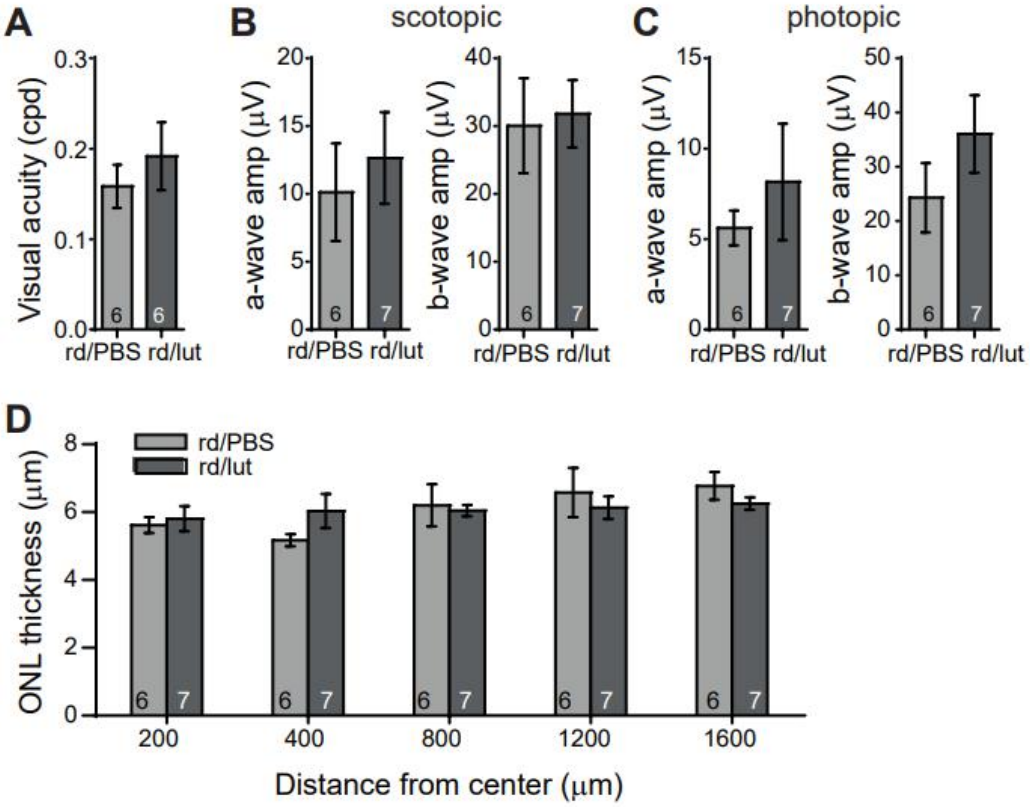

Additional Figure 1 Long-term effects of luteolin in rd10 mice.

(A) Average visual acuity for rd10 mice treated with PBS or luteolin until P25 and tested at P45. (B, C) Average amplitudes (amp) of the a- and b-waves in scotopic (B) and photopic (C) conditions. (D) Average ONL thickness from the center to the periphery. The improved ERG responses, ONL thickness or visual behaviors of rd10 mice were not persistent after the cessation of luteolin treatment at P25. Data are expressed as the mean ± SEM, and were analyzed by Student's t-test. The numbers within the bars indicate the quantity of mice tested. cpd: Cycle per degree; ERG: electroretinogram; ONL: outer nuclear layer; P: postnatal day; PBS: phosphate-buffered saline; WT: wild-type.

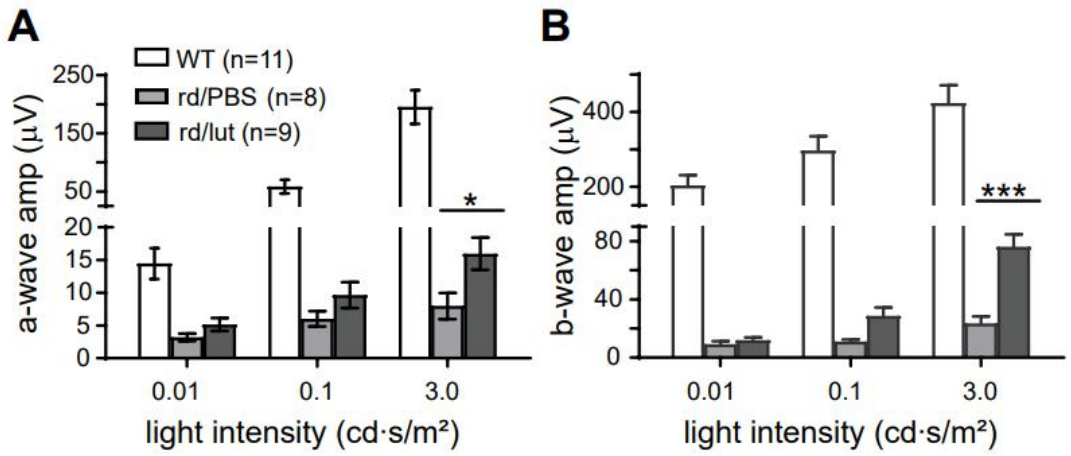

Additional Figure 2 Effects of luteolin on scotopic ERG responses at various flash intensities in rd10 mice.

(A, B) Peak amplitudes (amp) of scotopic a- (A) and b-waves (B) at flash intensities of 0.01, 0.1 and 3.0 cd·s/m² at P26. Data are expressed as the mean ± SEM. *$P < 0.05$, ***$P < 0.001$ (Student's t-test). The numbers of mice included in WT, PBS-treated and luteolin-treated rd10 groups are 11, 8 and 9, respectively. ERG: electroretinogram; P: postnatal day; PBS: phosphate-buffered saline; WT: wild-type.